First International Conference on SURFACE ENGINEERING Brighton, 25-28 June 1985

Vol. II
Weld Surfacing

Edited by Dr I.A. Bucklow
Conference Technical Director

Organised by The Welding Institute
in association with
The Surface Engineering Society

THE WELDING INSTITUTE

Fe-Cr-C hardfacing alloys for high-temperature applications

L.E.Svensson, B.Gretoft, B.Ulander and H.K.D.H.Bhadeshia

ABSTRACT

The microstructure and phase chemistry of a Fe-34Cr-4.5C wt.% hardfacing alloy have been investigated using transmission electron microscopy and microanalytical techniques. The microstructure is found to consist of large primary M_7C_3 carbides in a eutectic mixture of austenite and more M_7C_3. The results indicate that the microstructure of the undiluted alloy becomes configurationally frozen at a temperature of about 1150°C during deposition by the manual-metal-arc welding technique. This allows the metastable austenite phase to contain a large chromium concentration (about 16-17wt.%), thus imparting good corrosion and oxidation resistance. Experimental data on the partitioning of Cr, Mn and Si between the carbide phases are discussed in the context of the high-temperature stability of the alloy.

INTRODUCTION

Many common hardfacing alloys are based on iron, sometimes containing large additions of chromium and carbon. The present study is concerned specifically with the characterisation of a Fe-34Cr-4.5Cr wt.% alloy desposited by a manual metal arc welding technique. In this condition, the alloy contains a large volume fraction of hard, primary and eutectic chromium-rich carbides in a soft matrix. The carbides, which have a Vickers hardness of 1200-1600HV, provide resistance to wear by coarse sand and hard minerals and the austenite matrix seems to serve as a tough binder. The alloys are generally used at ambient temperature, but the high overall chromium content of the alloy should impart good corrosion and oxidation resistance to temperatures as high as 1000°C. Wear resistance should be maintained at high temperatures because, unlike tungsten carbide which readily decarburizes at temperatures greater than 500°C, the chromium carbide remains stable to beyond 1000°C. The overall hardness of the alloy is about 700HV.

The main aim of this study was to investigate whether the matrix phase (austenite, γ) contains enough Cr for adequate high-temperature corrosion and oxidation resistance, since much of the Cr in the alloy should be tied up in the form of carbides. For ambient temperature service in oxidising conditions, 12wt.% Cr is sufficient to form a continuous, adherent and selfregenerating Cr_2O_3 oxide film

which isolates the base metal from the environment. However, to provide adequate corrosion and oxidation resistance at temperatures near 1000°C, a higher Cr concentration of about 17wt.% is found to be necessary (1). Because of the fine-scale of the matrix phase in the microstructure, the investigation is carried out using microanalytical techniques associated with the transmission electron microscope.

EXPERIMENTAL DETAILS

Hardfacing alloys are usually deposited in three layers to avoid dilution of the top layer by the base material; thicker deposits can lead to extensive weld cracking. The welds are deposited using a manual metal arc welding technique with 4 mm diameter electrodes; the welding conditions are 160A, 23V AC with a deposition rate of about 0.004 m/s, the interpass temperature being 150°C. The bulk chemical composition of the final (top) layer was found to be Fe-4.46C-33.6Cr-1.19Mn-0.78Si-0.022S-0.028P (wt.%).

Thin foil specimens for transmission electron microscopy were prepared from 0.25 mm thick discs spark machined from the weld top layer deposits. The discs were subsequently thinned and electropolished in a twin-jet polishing unit using a 5 % perchloric acid, 25 % glycerol and 70 % ethanol mixture at ambient temperature and 55 V. The foils were examined in a Philips EM400T transmission electron microscope operated at 120 kV. Microanalysis experiments were also carried out on this microscope, using an energy-dispersive X-ray analysis facility. The specimens, which were about 100 nm thick in the areas of interest, were held in a beryllium holder tilted from the normal by 35° which is equal to the take off angle. The X-ray count rate was optimised to about 200 counts/s over a livetime of 100 s. The data were analysed using the LINK RTS 2 FLS program for thin foil microanalysis; this corrects the data for atomic number and absorption and accounts for overlapping peaks by fitting standard profiles. Even though the probe diameter used was about 3 nm, beam spreading due to scattering of electrons within the thin foil gave an estimated broadened beam diameter of 20 nm. This did not cause any difficulties since the scale of the microstructure is comparatively large. The elements analysed were Fe, Si, Mn and Cr; none of these cause significant fluorescence effects in thin foil samples. The absence of fluorescence or surface contamination layer effects was verified since microanalysis of regions of differing thickness within the same carbide particle gave very similar results. The error bars stated are those quoted by the LINK system and represent a conservative overestimate of the statistical error.

The beryllium window on the detector used in the microanalysis system absorbs X-rays from light elements so that C could not be analysed; this means that the microanalytical data have to be corrected for the presence of carbon. In the discussion that follows, y_i refers to the concentration of element "i" in weight percent, when the presence of carbon is ignored. The true concentration (wt.%) is denoted x_i; z_i refers to the ratio of the number of atoms

of i to the total number of substitutional atoms

It follows that for substitutional atoms,

$$y_i = 100w_i/(w_{Fe} + w_{Si} + w_{Mn} + w_{Cr}) \quad ...(1a)$$

where w_i is the weight of element i.

$$z_i = (y_i/A_i)/((y_{Fe}/A_{Fe})+(y_{Si}/A_{Si})+(y_{Mn}/A_{Mn})+(y_{Cr}/A_{Cr})) \quad 1b)$$

where A_i is the atomic weight of element i. The true concentration in wt.% is given by

$$x_i = 100\ w_i/(w_{Fe} + w_{Si} + w_{Mn}\ w_{Cr} + w_C) \quad ...(1c)$$

for a stoichiometric M_7C_3 carbide,

$$x_C = 300A_C/M \quad ...(1d)$$

where $M = 7(z_{Fe}A_{Fe} + z_{Cr}A_{Cr} + z_{Mn}A_{Mn} + z_{Si}A_{Si}) + 3A_C$,

and for the substitutional alloying elements we have

$$x_i = 700z_iA_i/M \quad ...(1e)$$

Similarly, if the carbon content of the austenite is known, then the corresponding x_i for γ can be calculated.

Most of the microanalysis work was carried out using transmission electron microscopy, but it proved difficult to obtain thin foil specimens containing the large primary carbides and their surrounding regions. These areas were therefore analysed in a scanning electron microscope fitted with a LINK energy dispersive x-ray analysis system; the LINK microanalysis program in this case corrected for fluorescence as well as atomic number and absorption effects.

RESULTS AND DISCUSSION

If the small amounts of Mn and Si are ignored, then the liquidus projection of the Fe-Cr-C system (Fig. 1a) indicates that primary M_7C_3 carbide is the first phase to form on cooling below the liquidus temperature; the residual liquid should then decompose via a ternary eutectic reaction into austenite and more M_7C_3 eutectic carbides. Consistent with this, optical microscopy shows the presence of large primary carbides which have a facetted morphology (Fig. 2). These primary carbides are assumed to be M_7C_3 carbides, consistent with the microanalytical results given in Table 1. They are surrounded by precipitate free zones, probably due to Cr depletion of the liquid in their vicinity - the γ near the primary carbides has a Cr level comparable to that of the eutectic austenite (Table 1), implying that it is not supersaturated with respect to the carbide phase. The remaining microstructure consists of a eutectic mixture of finer M_7C_3 carbides in an austenitic matrix, as confirmed by transmission electron microscopy and electron diffraction (Fig. 3).

The austenite was found to contain a large number of stacking faults (Fig. 3) and this is probably because chromium lowers the stacking fault energy of austenite (2). M_7C_3 has a complex hexagonal lattice ($D10_1$ structure, with a=1.398 nm and c=0.451 nm for M_7C_3 of present composition (3) and the resulting small c/a ratio means that the basal plane is not close-packed. Faulting therefore usually occurs on the prism planes; the eutectic M_7C_3 always appeared streaked (Fig. 3) and this is believed to be due to such faulting.

The results from microanalysis experiments on the eutectic structure are presented in Fig. 4 and the mean concentrations are summarised in Table 1. The carbon content of the carbide is deduced assuming stoichiometry and that of the austenite is estimated from the Fe-Cr-C phase diagram, as discussed later.

Focussing now on the eutectic regions, neither the γ nor the M_7C_3 showed significant composition variations between the different regions analysed. This is probably because both the M_7C_3 and γ (of the eutectic) can co-exist over a narrow composition range; in Figs. 1b-d, the lines zy and wx represent the possible M_7C_3 and austenite (or ferrite) compositions respectively. The Fe content of the M_7C_3 carbide was in all cases found to be consistent with the fact that M_7C_3 is known (4) to dissolve up to 55 wt.% of iron, and the carbide clearly rejects silicon (Fig. 4) while Mn preferentially partitions into the carbide phase. The austenite on average contains 16.4 wt.% Cr (lightly lower than the γ near the primary carbide) and this is just adequate to provide corrosion and oxidation resistance at high temperatures.

In the discussion that follows, the presence of small amounts of Mn and Si in the alloy are ignored, the microstructure being discussed in terms of the Fe-Cr-C phase diagram. In each of Figs. 1b-d, the point x defines the maximum Cr content possible in the eutectic γ or α (henceforth referred to as x^m_{Cr}), when either of these phases is in equilibrium with M_7C_3. x^m_{Cr} clearly decreases with decreasing temperature. The microanalysis results (Fig. 4, Table 1) and the fact that the matrix phase is γ (rather than α) strongly suggests that the as-desposited microstructure is far from equilibrium. The equilibrium microstructure of the alloy is in fact α+M_7C_3, as illustrated in Fig. 1d. Even at 1150°C, x^m_{Cr} = 15.1 wt.%, whereas it is experimentally found that the γ contains about 16.4 wt.% Cr. The observed microstructure is therefore configurationally frozen at some temperature just above 1150°C, and it is this structure which is retained to ambient temperature without further change. All this is a consequence of the high cooling rates involved in manual metal arc welding and the fact that all of the transformations necessary to accomplish equilibrium require thermally activated, long-range diffusion. The experimentally determined partition coeffient k_{Cr} = 3.4 (ratio of x_{Cr} in M_7C_3 to that in γ, Fig. 4) is also consistent with reactions stopping at T>1100°C (Fig. 4). The melting point of the alloy is about 1380°C, so that the entire microstructure can be considered to have formed within the narrow temperature range 1380-1150°C.

The phase diagrams indicate that service at temperatures between 850-1150°C must lead to a gradual equilibration of the system, with a decrease in the γ Cr content. Extended service at lower temperatures (e.g., 700°C) must cause the γ to diffusionally transform to α with a further decrease in matrix Cr concentration. These changes are thermodynamically favoured, but the time scale over which they occur is a function of kinetics, and initial experiments suggest that the changes might be very sluggish, since they involve long-range substitutional atom diffusion. Preliminary results indicates that the alloy only seems to undergo significant oxidation at temperatures round 1050°C. This resistance to oxidation is probably a result of the high amount of carbide phase in the microstructure, containing some 55 wt.% of Cr.

CONCLUSIONS

The Cr concentration of the austenite matrix of Fe-34Cr-4.5C wt.% hardfacing alloy is sufficiently high to provide oxidation and corrosion resistance at high temperatures. The microstructure of the alloy, as deposited by a manual metal arc welding technique, is that retained from a temperature just above 1150°C. The as-deposited $M_7C_3 + \gamma$ microstructure is thus metastable, and given sufficient thermal activation, should tend to equilibrate. Equilibration could involve a reduction in the Cr content of the γ (T>700°C), or the decomposition of γ into α (with lower Cr content) and M_7C_3 at temperatures around 700°C. The kinetics of the equilibration processes are not known and require further investigation. The work indicates that the alloy has good potential for high temperature applications.

ACKNOWLEDGMENTS

The authors are grateful to ESAB AB (Sweden) for financial support and for the provision of laboratory facilities, and to Professor D. Hull for the provision of laboratory facilities at the University of Cambridge. Helpful discussions with Dr. A.J. Bourdillon on aspects of microanalysis are gratefully acknowledged.

REFERENCES

1) SCULLY J.C., "The Fundamentals of Corrosion", 2nd ed., Pergamon Press, Oxford, 1981, p. 45.
2) SCHRAMM R.E. and REED R.P., "Stacking fault energies of Seven Commercial Austenitic Stainless Steels". Metall. Trans. A, Vol. 6A, July 1975, pp. 1345-1351.
3) DYSON D.J. and ANDREWS K.W., "Carbide M_7C_3 and its formation in alloy steels". J.I.S.I., Vol. 207 (1969), pp. 209-219.
4) Metals Handbook, Vol. 8, American Society for Metals, Ohio, USA, 1973, p. 402.
5) B. UHRENIUS, "Hardenability Concepts with Applications to Steel", Eds. D.V. Doane and J.S. Kirkaldy, Met. Soc. AIME, USA, 1977, p. 28.

TABLE 1

Mean compositions of eutectic phases (error estimates can be obtained from Fig. 4). The results are quoted to two decimal places for internal consistency. The carbon concentrations are deduced as discussed in the text. The results for the primary carbides and the austenite around the primary carbides are obtained using scanning electron microscopy, and represent the mean of two tests in each case (the errors are comparable to those illustrated in Fig. 4).

	Eutectic γ		Eutectic M_7C_3		Primary M_7C_3		γ near Primary M_7C_3	
	y_i	x_i	y_i	x_i	y_i	x_i	y_i	x_i
Fe	80.64	80.29	37.21	33.94	42.40	38.68	77.76	77.41
Si	1.70	1.69	0.18	0.16	0.18	0.16	1.86	1.85
Mn	1.15	1.14	1.56	1.43	0.99	0.90	1.39	1.38
Cr	16.51	16.43	61.05	55.67	56.43	51.47	18.99	18.91
C		0.45		8.80		8.78		0.45

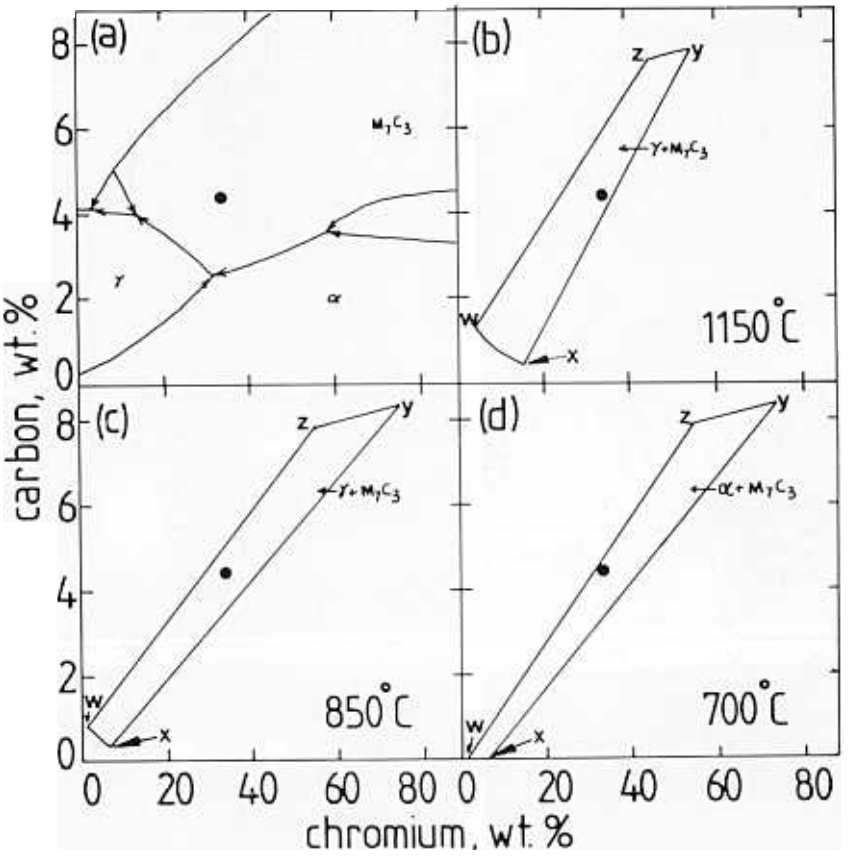

Fig. 1

a) Liquidus projection of the Fe-Cr-C system (1).
b-d) the γ+M_7C_3 or α+M_7C_3 phase fields (wxyz) in isothermal sections of the Fe-Cr-C system (1). The approximate composition (i.e., ignoring Mn, Si) of the alloy used is indicated (•) in each figure.

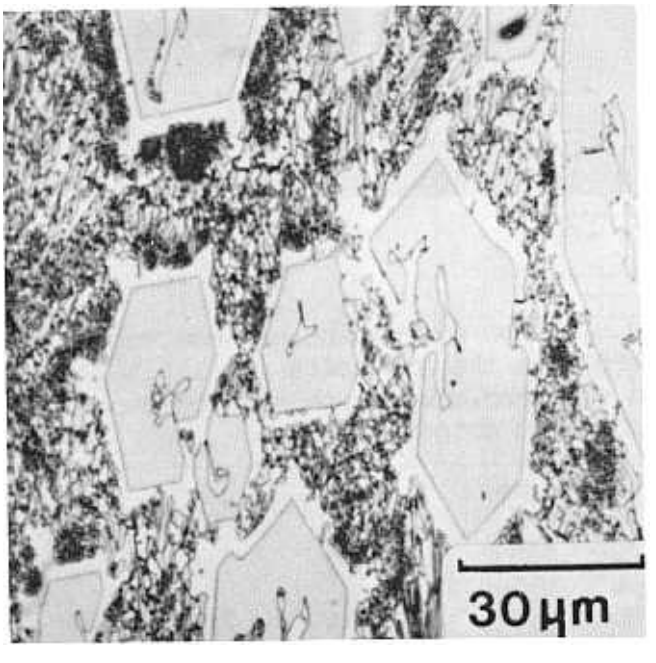

Fig. 2

Optical micrograph of the top layer.

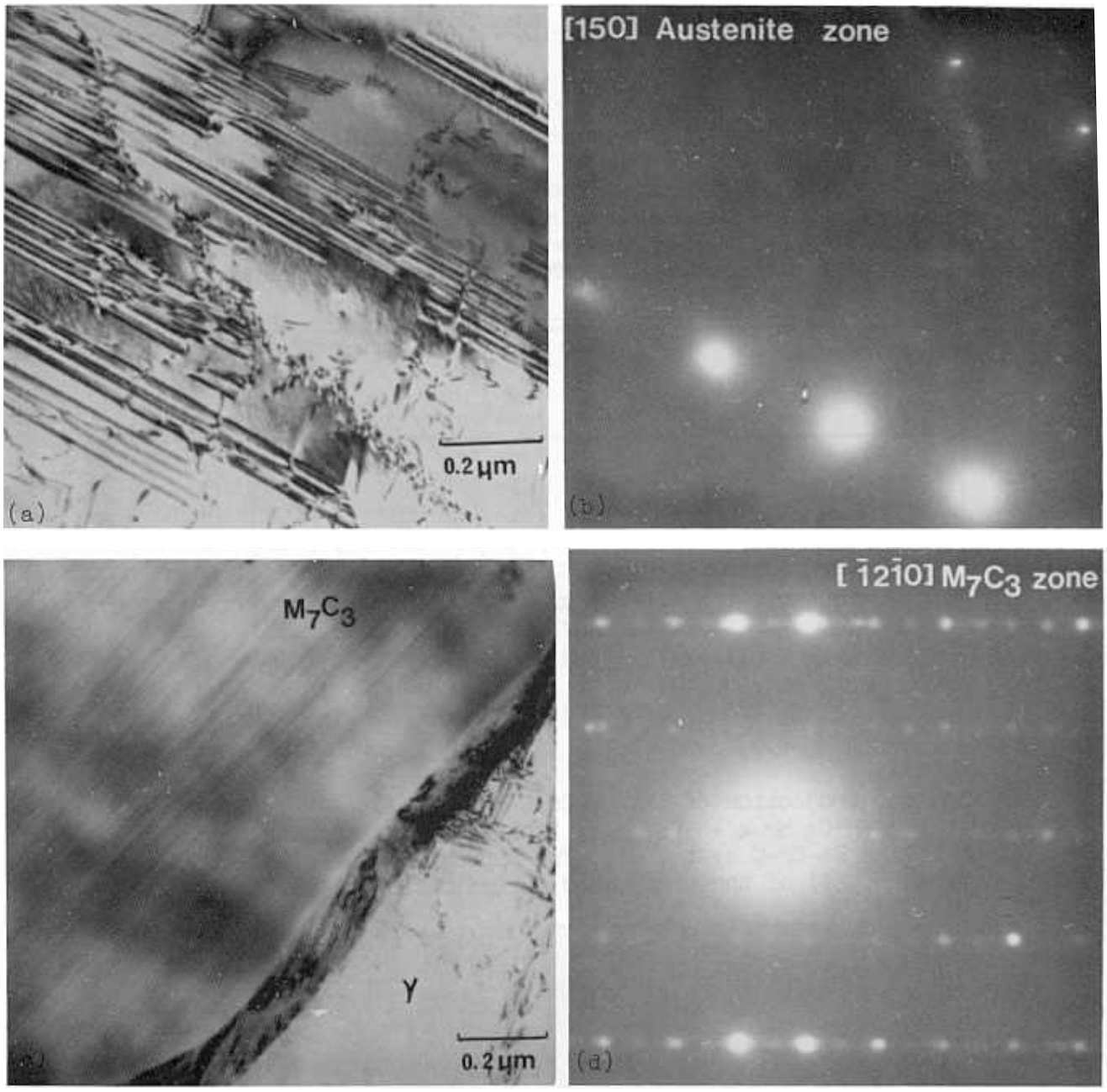

Fig. 3

a-b) Transmission electron micrograph and corresponding electron diffraction pattern from the austenite matrix.
c-d) Transmission electron micrograph and corresponding electron diffraction pattern from eutectic M_7C_3.

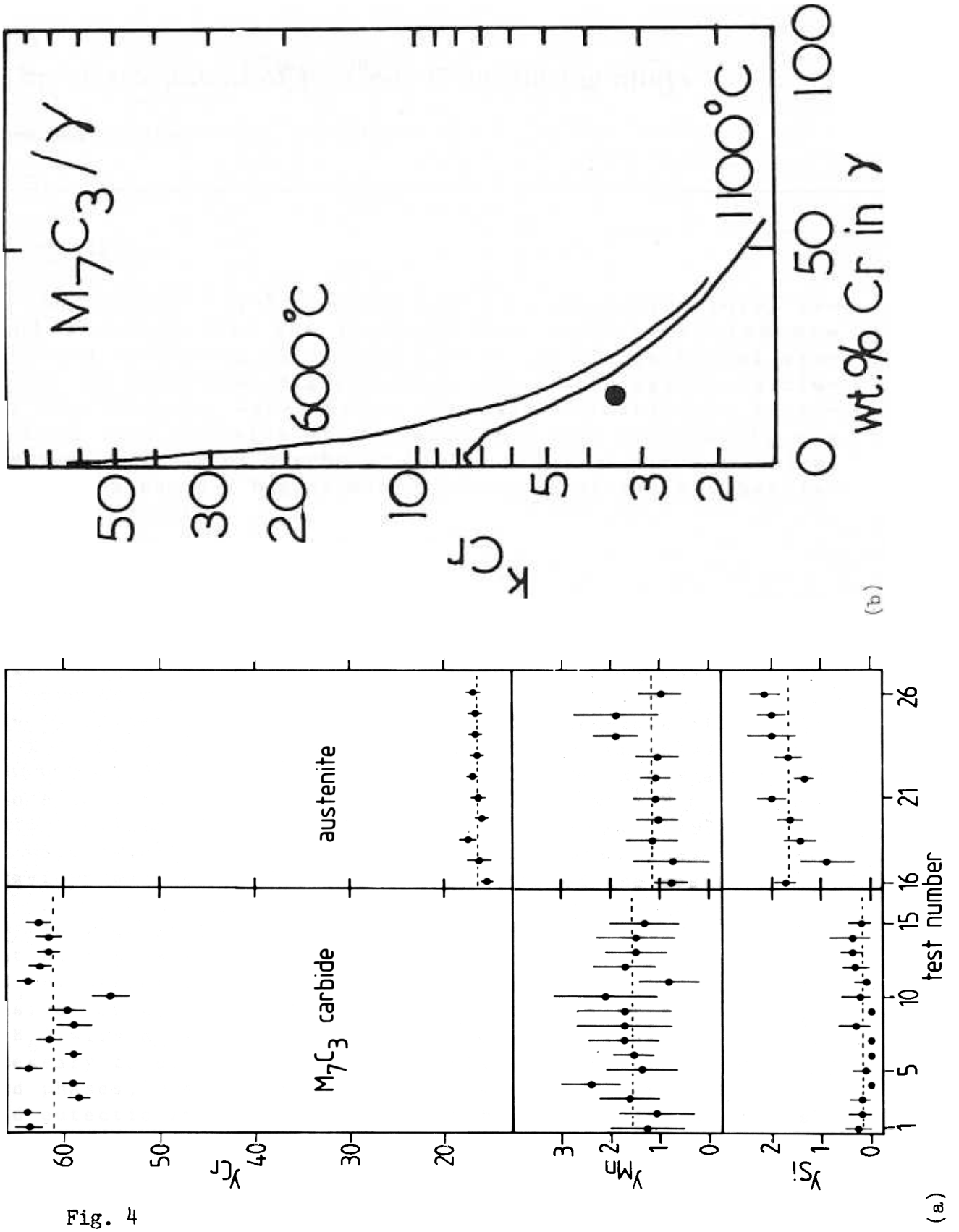

Fig. 4

a) Microanalytical (TEM) data on eutectic M_7C_3 and γ phases (y_i has units of wt.% and is defined in eq.1a).
b) Partitioning coefficients for the Fe-Cr-C system (5). The partitioning coefficient for the experimental alloy (•) indicates that the as-deposited microstructure is frozen from about 1150°C.